B&H Electrical Engineering, Volume 20, Issue 1, 2026
ISSN:2566-3143, eISSN:2566-3151, DOI: 10.2478/bhee-2026-0019

DEPENDENCE OF UHF PARTIAL DISCHARGE DETECTION AND SOURCE POSITIONING IN POWER TRANSFORMERS ON DIFFERENT INPUT PULSE FREQUENCY RANGES

Đorđe Dukanac[1,2]

Abstract: Transformer insulation is gradually weakened by partial discharges (PDs), which might eventually result in complete transformer failure if left unchecked. Different types of sources can produce PD signals, which can be detected throughout a wide frequency range. Preventive maintenance of power transformers depends on the characteristics of received ultra-high frequency (UHF) PD signals at sensors and the positioning of their source. This study compares and analyses the effects of different input pulse frequency ranges (IPFRs), the transformer tank, the active components of the transformer, dispositions of UHF sensors relative to PD source, the total efficiency of the used antenna and superimposed reflected waves on received signals' waveforms, times of arrivals (TOAs) and magnitudes of their first peaks (FPs), time differences of appearances and magnitude ratios between the extreme amplitudes and FPs in their first wave packets, as well as variations in their amplitude spectra.

Keywords: Input Pulse Frequency Range (IPFR), First Peak (FP), Partial Discharge (PD), PD source, power transformer, Time Difference of Arrival (TDOA), Time of Arrival (TOA), Ultra-High Frequency (UHF)

INTRODUCTION

Electrical power transmission and distribution systems depend heavily on power transformers. The insulation of power transformers ages with time, and anomalous environmental activities, including mechanical, electrical, and chemical stressors, hasten this process. Partial discharge (PD), a localized breakdown of insulation materials in power transformers, is a significant problem that can lead to catastrophic failure if not detected in time. Released energies from PDs, such as light, heat, and electromagnetic waves, are prevented from passing through the metal case, so they must be detected by the internal sensor [1]. It is frequently challenging to detect and locate PD, and the ultra-high frequency (UHF) method is one of the diagnostic techniques that has been developed. The insensitivity to on-site external noises is one benefit of operating under the ultra-high frequency (UHF) band [2].

The frequency spectrum for PD measurements using the UHF method in power transformers, according to Cigré TB 861, ranges from 100 MHz to 1 GHz, and more recently, from 400 MHz to 900 MHz [3,4]. Uncertainties remain regarding the frequency range that PDs radiate and the frequency range that must be assessed in a measurement [5]. According to one example of online UHF PD monitoring of a repaired 40 MVA, 123 kV substation transformer using two UHF antennas, which were mounted on two DN80 oil gate valves, the frequency ranges above 600 MHz were significantly more attenuated for UHF sensor 2 than for UHF sensor 1. It could be because UHF sensor 2 is farther away from the PD source than UHF sensor 1. It was suggested that a wider range is preferable, since the actual PD signal peak of an individual case can be outside this range, between 400 MHz and 900 MHz. The table of influence of the type of antenna and test object on the frequency parameters of PDs is shown in [5].

In [6], four UHF sensors installed on the transformer tank were used to identify the position of the PD source. At every power transformer's UHF sensor, the received PD signal is influenced by the following factors [2]:

- The power transformer's internal structure, which usually determines the quickest path for VHF/UHF waves to travel between the PD source and the UHF sensor
- The transformer tank's resonant cavity, which permits certain resonant modes with powers for specific frequencies based on its size
- The location of the PD source and its specific type
- The sensor's location, its radiation pattern, polarisation, and frequency response

The complex solid structure of the transformer windings and the presence of mineral oil in the transformer tank make it challenging to temporarily install an antenna

[1] Joint Stock Company "Elektromreža Srbije", Serbia
[2] Correspondence email: djordje.dukanac@ems.rs

(supplied by an artificial pulse generator) as the artificial source for the PD signals' emission to conduct PD detection investigations on a real power transformer. In [7], for instance, twenty-four holes were drilled into the transformer tank to install the monopole antennas, and four antennas were used to act as PD sources. For these reasons, simulations of the propagation of PD signals through the internal structure of the transformer and the positioning of their source in the transformer model are highly suitable solutions. [8] presents a study that uses the FDTD method to investigate the propagation of UHF PD signals in power transformers. In the middle of a tank, two different obstacles—a conducting cylinder and a cuboid—were placed in turn. Several power transformer models, ranging in complexity from simplified to composite, were employed in [1,9] to provide simulation results for the detection of PD signals at four UHF sensors. The attenuations of the PD-EM waveforms received at the UHF sensors were influenced by the receiving antennas' imperfect orientations and positions relative to the transmitter (PD source). In [10], it was demonstrated how to obtain more realistic signals utilising a specific technique and MATLAB simulation.

In [11,12], the CST (Computer Simulation Technology) microwave studio was utilised to model a power transformer with a PD source and UHF antennas and to simulate the propagation of PD signals. In [11], Dijkstra's algorithm was used for pathfinding. The pathfinding procedure required a voxelised 3D simulation model of the transformer, and a database of time differences of arrivals (TDOAs) was built to act as a lookup table for measured TDOAs for localisation. In [12], machine learning and deep learning techniques were employed to investigate PD localisation using three sensors on a simplified steel transformer tank model.

Results of PD source location in the power transformers gained in the various simulations in the literature, like in [11,12], depend on actual PD source location relative to the UHF sensors, the size and complexity of the transformer model, and the PD signal pulse frequency range, so they cannot be simply comparable with the results in this paper.

This study aims to analyse and compare how various frequency ranges of the PD source input pulse, along with transmitting and receiving antennas' total efficiency and the internal transformer structure, affect signal characteristics at each of the four sensors (such as waveforms, first peaks (FPs), extreme amplitudes, amplitude spectra), as well as PD source positioning. These are both significant for the power transformer's preventive maintenance. Therefore, those simulations of the propagation of PD UHF signals and the subsequent positioning of a PD source are beneficial. The simulation model is described in Section 1. Section 2 explains how the detected PD signals and the PD source location in power transformers depend on several pertinent input pulse frequency ranges (IPFRs). The conclusion is presented in Section 3.

1. SIMULATION MODEL

Ansys HFSS and a typical three-phase power transformer model were used to simulate the propagation of signals from the PD source to four UHF sensors in order to do in-depth research. Figure 1a and Figure 1b display the trimetric and top layouts of the models, respectively. The transformer model had a stainless steel 304 tank filled with mineral oil, a three-phase low voltage (LV) and high voltage (HV) copper windings, and a three-limb four-step electrical steel magnetic core. Four UHF sensors and a PD source were modelled using five dipole antennas.

Given the tank's dimensions of 2800 mm in height, 880 mm in width, and 2300 mm in length, a small three-phase power transformer with a 66/11 kV transformation ratio and a 5 MVA total deliverable apparent power was considered. S_1 = (65, 65, 2750) mm, S_2 = (1150, 440, 2758) mm, S_3 = (2235, 815, 2755) mm, and S_4 = (70, 810, 2760) mm were the locations (centres of masses) of the receiving UHF antennas. The transmitting antenna, which acted as the PD source, was assumed to have a centre of mass at O = (1985, 295, 1485) mm. It was situated at the upper portion of the first phase of the winding, on the rear side of the first limb of the core. It was positioned nearer the LV winding, between the 37th and 38th disks of the LV winding, and nearer the magnetic core, as shown in Figure 1a and Figure 1b. Figure 1c displays the 60 mm by 5 mm copper-based dipole antenna arms with a 4 mm by 5 mm port positioned in between.

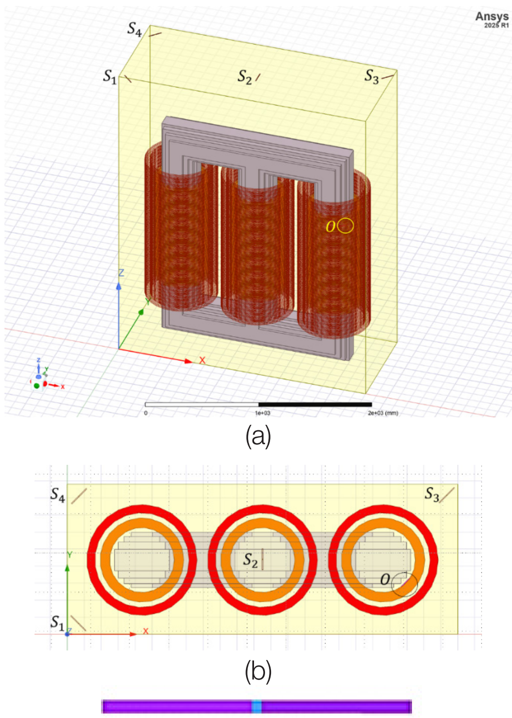

(a)

(b)

(c)

Figure 1: (a) Trimetric layout of the transformer model with five antennas (S_1, S_2, S_3, and S_4 are the UHF sensors, and O is the PD source). (b) The top layout of the transformer model. (c) The dipole antenna model.

ISSN:2566-3143, eISSN:2566-3151, DOI: 10.2478/bhee-2026-0019

1.1. Model limitations and simplifications

Due to the limited capabilities of the computer (primarily the processor, random-access memory (RAM), and SSD memory as well) and the complexity of Ansys HFSS software and its calculations, a couple of necessary simplifications and limitations of the power transformer construction were made to perform simulations. Firstly, the inter-insulation between adjacent turns of each of the 42 corresponding LV or HV discs in the radial direction, with a thickness of 1.2 mm, is not considered and is assumed to be copper. Each HV disk is divided into two parts along the vertical axis with a gap of 1.2 mm, although it should be composed of four parts. Neglecting the two 1.2 mm vertical gaps in each HV winding's disk results in a slightly larger signal attenuation. EM waves in mineral oil (with the dielectric constant of $\varepsilon_r = 2.2$) have a wavelength of 15.51 cm at 1.7 GHz and 24.17 cm at 700 MHz; thus, 1.2 mm is a tiny aperture for these waves. Every wave diffraction at such a small aperture causes the wave beam passing through it to lose intensity in different directions relative to the aperture itself, which results in a loss in signal strength from the PD source in the path shortest to a particular UHF sensor.

Secondly, the paper insulation and the pressboard inter-insulation of the three-phase LV and HV windings were considered to be mineral oil since they are both impregnated with mineral oil, which lowers their dielectric constant. Thirdly, due to the lack of precise data and the additional complexity of the power transformer model, the following less present and influential parts were not considered: a) insulating parts such as insulating spacers, strips, bushings, etc. and b) metal parts, including screws, winding fixing parts, core clamping frames, windings' leads, etc.

1.2. 3D total gain polar diagrams of the transmitting antenna for different frequencies

In Figure 2, the transmitting dipole antenna is assumed to be located within a cube with transparent walls (i.e., a radiation boundary) filled with mineral oil, with a side length of 400 mm, to facilitate simulations and create 3D polar diagrams of the PD source's total gains for different frequencies for comparison. The PD pulses were simulated using broadband Gaussian pulses with an amplitude of 1 V for the following IPFRs of: [0–0.7] GHz, [0–1] GHz, [0–1.5] GHz, and [0–1.7] GHz.

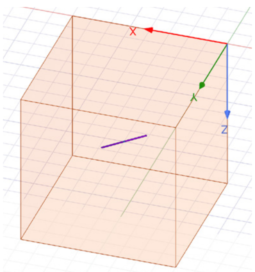

Figure 2: A dipole antenna in a cube with transparent walls.

IPFRs were chosen in very different ranges to make a better comparison between them. In Figures 3a-d, the 3D polar diagrams of the UHF dipole antenna's total gains, expressed in decibels [dB], were respectively obtained at 700 MHz, 1 GHz, 1.5 GHz, and 1.7 GHz. Due to the transmitting dipole antenna's design, the 3D polar diagrams of its total gains, as seen in Figures 3a-d, significantly depart from the optimal spherical forms at the frequencies taken into consideration. A significantly greater number of zones of lower intensity of total gains are in the middle of the polar diagrams in the plane of the dipole antenna in the longitudinal direction of the antenna. The 3D polar diagrams' surfaces become less smooth as the PD source radiation frequencies increase. On the 3D polar diagrams, the largest and the smallest maximum values of the PD source total gains are respectively 2.36 dB at 1.5 GHz and -1.79 dB at 700 MHz.

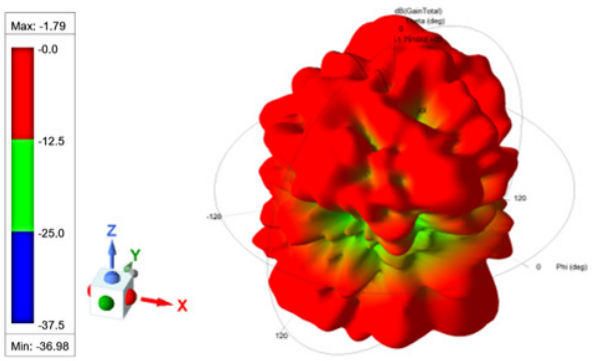

(a)

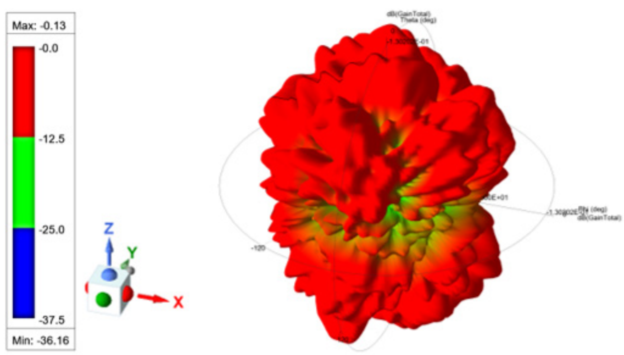

(b)

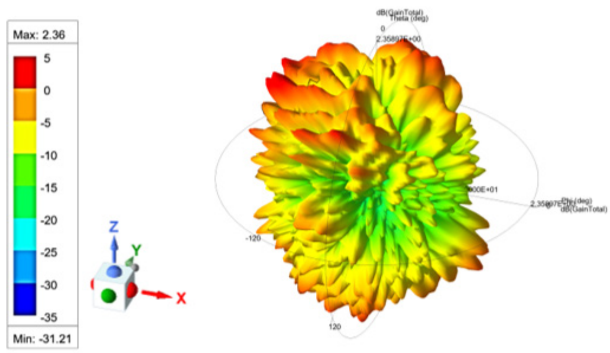

(c)

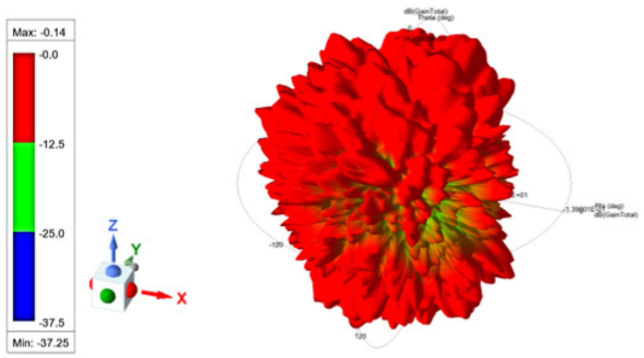

(d)

Figure 3: 3D polar diagrams of the PD source in trimetric orientation showing the total antenna gains in [dB] for different frequencies: (a) 700 MHz, (b) 1 GHz, (c) 1.5 GHz, (d) 1.7 GHz.

In this paper, supposing a y-frequency graph, the term weighted average frequency ($\bar{f}$) is used, which is given by:

$$\bar{f} = \frac{\sum_{i=1}^{n} f_i \cdot y_i}{\sum_{i=1}^{n} y_i} \quad (1)$$

Where y_i is the i-th magnitude at the y-axis, which is taken as a weight assigned to the i-th frequency f_i. Weighted average frequencies are important for comparing the results of analyses for various IPFRs. These will be obtained from the receiving antennas' total efficiency graph in this Section and the amplitude spectra of 1) the transmitting antenna's input pulses, 2) the transmitting antenna's output signals, and 3) the recorded signals from receiving antennas (i.e., UHF sensors) in Section 2.

The total antenna efficiency for the [0–1.7] GHz IPFR is displayed in Figure 4, utilising a frequency sweep in 601 points derived from the simulation, which was run using the model in Figure 2. Therefore, the antenna's total efficiency peak of 0.97 appears at 750.9 MHz in the [0–1.7] GHz IPFR. The total efficiency of the antenna is larger than 0.5 in the frequency range of [614.9–1034.2] MHz. For the IPFRs of [0–0.7] GHz, [0–1] GHz, [0–1.5] GHz, and [0–1.7] GHz, the weighted average frequencies are 613.4 MHz, 768.5 MHz, 937 MHz, and 1007.5 MHz, respectively. The radiation efficiency of an antenna is defined as the ratio of the power radiated by an antenna to the power fed to the excitation port of the antenna. Total radiation efficiency also includes the power lost due to poor voltage standing wave ratio (VSWR) (or mismatch loss). It is a multiplication of antenna efficiency and mismatch loss.

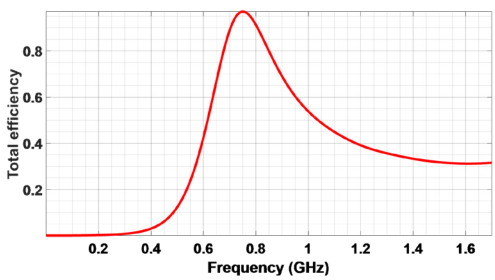

Figure 4: Total efficiency of the transmitting antenna versus frequency.

The same 3D polar graphs of total gains for various frequencies and the total efficiency vs frequency diagram in the [0–1.7] GHz IPFR are likewise useful for the receiving antennas that have the same properties as the transmitting antenna.

2. RESULTS

Simulations were run using the finite element method (FEM) in Ansys HFSS. The reflections of all PD waves off the transformer tank walls, three-phase LV and HV windings, and three-limb magnetic core were considered. Also taken into consideration were all PD wave diffractions around the active metal components (copper windings and magnetic core), as well as through the tiny gaps between the metal components of the LV and HV coils of the core-type transformer.

2.1. Analysing input pulses and output signals at the PD source for various IPFRs

As will be shown later, the output signals at the sensors depend mainly on the characteristics and mutual orientations of the antennas, IPFRs, the internal structure of the transformer, and the line-of-sight (LOS) distances between the PD source and the sensors.

Figure 5a shows the positive input broadband Gaussian pulses at the transmitting antenna, serving as the PD source, for different IPFRs of: [0–0.7] GHz, [0–1] GHz, [0–1.5] GHz, and [0–1.7] GHz, with an amplitude of 1 V. As the IPFRs expand, the pulses have earlier peaks and smaller widths, with mutual ratios of their times of peaks' appearances and pulse widths roughly proportionate to the mutual ratio of their respective frequency ranges.

Figure 5b shows corresponding amplitude spectra gained from the input pulses in the periods of [0.8–4.6] ns, [0.4–3.4] ns, [0.2–2.2] ns, and [0–2] ns, respectively. From Figure 5b, the weighted average frequencies of the four input pulses for different IPFRs of [0–0.7] GHz, [0–1] GHz, [0–1.5] GHz, and [0–1.7] GHz are 196.7 MHz, 503.1 MHz, 652.9 MHz, and 467.7 MHz, respectively.

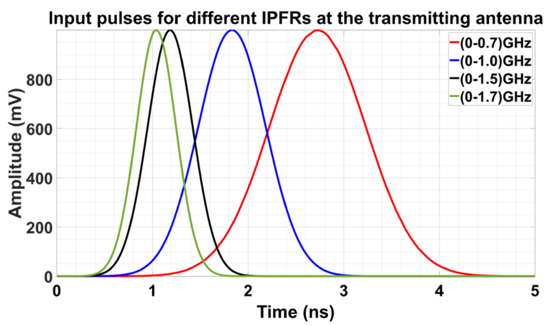

(a)

ISSN:2566-3143, eISSN:2566-3151, DOI: 10.2478/bhee-2026-0019

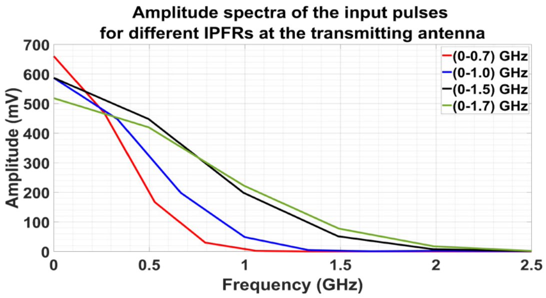

(b)

Figure 5: (a) Input Gaussian PD pulses for the different IPFRs at the transmitting antenna. (b) Corresponding amplitude spectra of the input pulses.

Figure 6 shows signals at the output port of the transmitting antenna for the different IPFRs. In contrast to the corresponding positive input Gaussian pulses in Figure 5a, all output signals at the transmitting antenna exhibit oscillations after the completion of their positive initial pulses. Higher IPFRs result in correspondingly smaller peaks, more delayed peaks, and larger deformations of the peaks of the output excitation signals' positive initial pulses. They also cause larger and more frequent oscillations following the ends of their positive initial pulses. Even the positive initial pulses of the output signals for IPFRs of [0–1.5] GHz and [0–1.7] GHz exhibit oscillations at their peaks, making them significantly wider than the corresponding positive input Gaussian pulses.

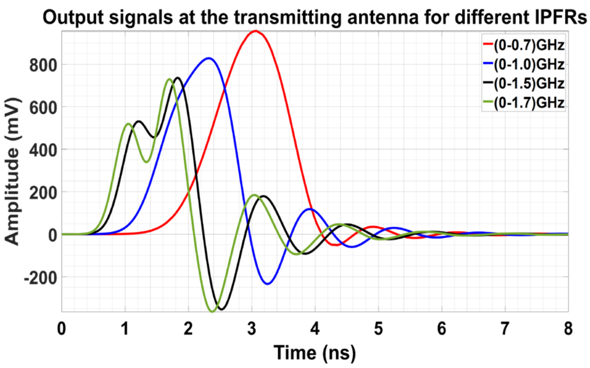

Figure 6: Output signals at the transmitting antenna for different IPFRs.

Figure 7 shows the time differences of appearances and magnitude differences between the extreme peaks of the output signals' initial pulses (from Figure 6) and the corresponding maximal peaks of the input pulses (from Figure 5a) at the transmitting antenna for different IPFRs. It can be seen that as IPFR increases, the extreme peak of the output signal's initial pulse is more delayed and has a decreased magnitude relative to the respective maximal peak of the input pulse at the transmitting antenna. The time difference of appearance and magnitude difference are 6.26 and 2 times higher than at [0–0.7] IPFR, 1.57 and 1.34 times bigger than at [0–1] GHz IPFR, and 1.025 and 1.023 times higher than at [0–1.5] GHz IPFR, respectively, in comparison to [0–1.7] GHz IPFR.

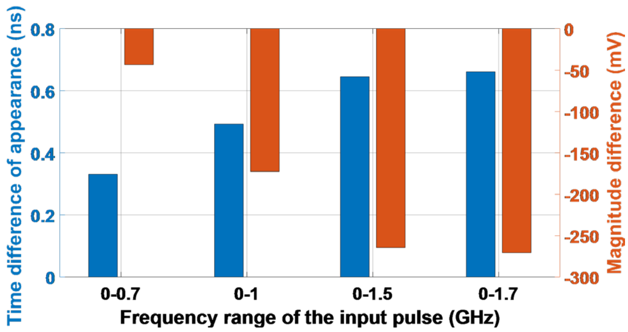

Figure 7: Time differences of appearances and magnitude differences between the extreme peaks of the output signals and the corresponding input pulses at the transmitting antenna, for different IPFRs.

The amplitude spectra of the output signals at the transmitting antenna for the different IPFRs of [0–0.7] GHz, [0–1] GHz, [0–1.5] GHz, and [0–1.7] GHz are shown in Figure 8, in the periods of the output signals of [0.8–8.0] ns, [0.4–8.0] ns, [0.2–8.0] ns and [0–8] ns, respectively. As the IPFR of the PD source is higher, the amplitude spectrum of the output excitation signal is wider, but its peak value is lower. The maximal peaks in Figure 5b's input pulse amplitude spectra at the transmitting antenna are larger than the corresponding maximal peaks in the amplitude spectra of the output excitation signals [1.9, 2.5, 3.7, and 3.9 times].

From Figure 8, the weighted average frequencies of the four output excitation signals for different IPFRs of [0–0.7] GHz, [0–1] GHz, [0–1.5] GHz, and [0–1.7] GHz are 230.8 MHz, 423.2 MHz, 582.8 MHz, and 568.9 MHz, respectively. In comparison to the weighted average frequencies of the four input pulses, the differences are 34.1 MHz, -79.9 MHz, -70.1 MHz, and 101.2 MHz.

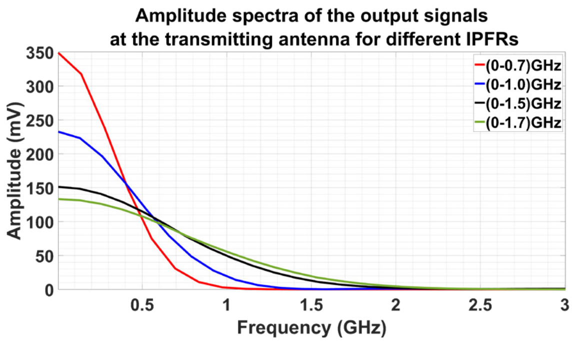

Figure 8: Amplitude spectra of output signals at the transmitting antenna for different IPFRs.

A portion of the PD source power, which is reflected to the antenna from the adjacent metal components of the transformer, causes oscillations, smaller peaks, and different weighted average frequencies in the output excitation signals compared to the corresponding input pulses. Consequently, modifications have been made to the input PD pulse's spectrum characteristic, which may impact its classification or diagnostic application.

2.2. Analysing signals at UHF sensors originating from PD source output pulses for various IPFRs

The PD output excitation signals had to travel via a complex transformer internal construction (simulated in the model) to reach the UHF sensors. During this process, they encountered many diffractions and reflections, all of which were captured by running simulations.

The output received signals at sensors 1, 2, 3, and 4 are respectively displayed in Figures 9a-d, for the various IPFRs of [0–0.7] GHz, [0–1] GHz, [0–1.5] GHz, and [0–1.7] GHz. One may observe that the first wave packet width of signal 1 is approximately 10 ns, that of signal 2 is about 12.4 ns, that of signal 3 is roughly 9.4 ns, and that of signal 4 is approximately 10 ns. Since the signals initially emerged at the sensors, they have been impacted in diverse ways throughout time by the reflected signals from the metal components of the transformer's internal structure. Consequently, only the effects of reflected waves may be attributed to portions of the received signals that extend beyond their first wave packets.

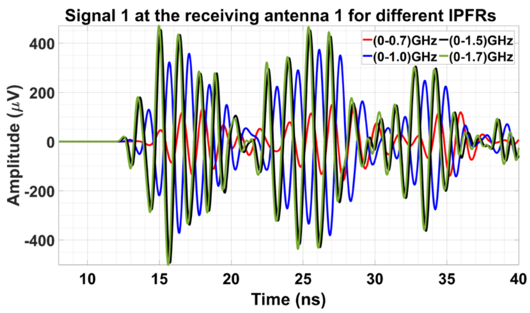

(a)

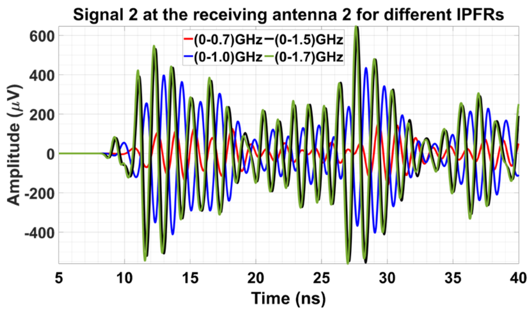

(b)

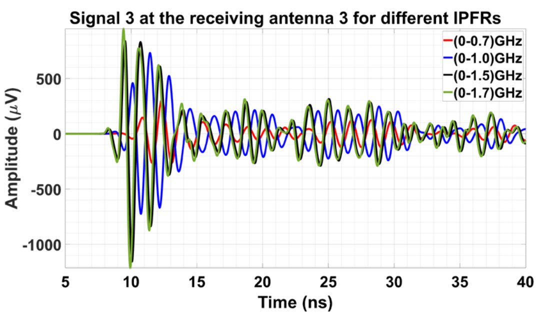

(c)

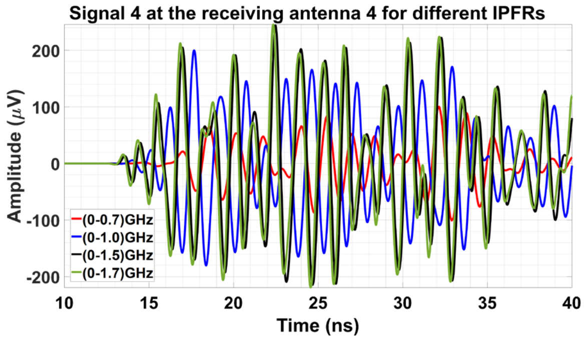

(d)

Figure 9: Output signals recorded at sensors (a) 1, (b) 2, (c) 3, and (d) 4, for different IPFRs.

Signal 4 is the most attenuated and has the most pronounced impacts from reflections because it had to take the longest and most convoluted path across the internal transformer construction. In signals 2 and 4, extreme amplitudes in the periods from the end of the first packets to 40 ns even exceeded the extreme amplitudes of the signals' first wave packets. In contrast, signal 3 is the least attenuated and contains the lowest impacts of reflections because it had to take the simplest and shortest path via the internal transformer construction.

Figure 10 shows all recorded signals FPs' times of arrivals (TOAs) at four UHF sensors for different IPFRs. The TOAs of FPs of all signals at sensors are, as anticipated, largest in the [0–0.7] GHz IPFR and decrease as the IPFR increases. For each IPFR, the TOAs of FPs of all signals at sensors depend mainly on the positions of the sensors relative to the PD source.

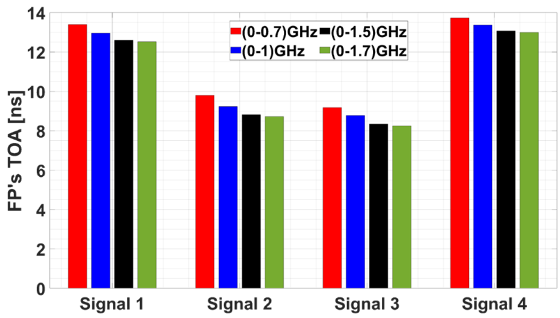

Figure 10: FPs' TOAs of recorded signals 1–4 at four UHF sensors for different IPFRs.

The LOS distances between the PD source and the UHF sensors 1, 2, 3, and 4 are 2.31 m, 1.53 m, 1.39 m, and 2.36 m, respectively. However, in the simulation model in Figure 1a, the corresponding distances could be larger because they also depend on the metal obstacles along the shortest paths from the PD source to the sensors. For example, the LOS distance ratio or ideal ratio of TOAs of the FPs of signals 3 and 4 is 1.7. However, the corresponding ratio is smaller in the simulations based on the model in Figure 1a, and for the various IPFRs of [0–0.7] GHz, [0–1] GHz, [0–1.5] GHz, and [0–1.7] GHz, respectively equals, 1.5, 1.52, 1.57, and 1.58.

ISSN:2566-3143, eISSN:2566-3151, DOI: 10.2478/bhee-2026-0019

Figure 11 shows the FPs' magnitudes of recorded signals at four UHF sensors for different IPFRs. Because there are the most metal obstacles on the path from the PD source to sensor 4, signals recorded at sensor 4 have the lowest FPs for all four IPFRs.

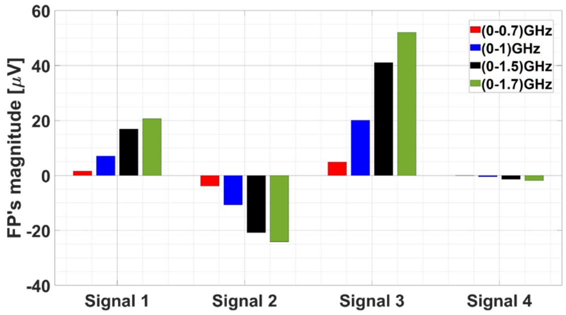

Figure 11: FPs' magnitudes of recorded signals at four UHF sensors for various IPFRs.

Sensor 1's LOS distance from the PD source is similar to that of sensor 4. Compared to sensor 4, the LOS distance between the PD source and sensor 1 is just 1.02 times shorter. However, because there are significantly fewer metal obstacles between the PD source and sensor 1 than between the PD source and sensor 4, the recorded signals FPs are considerably larger, or in the range of [11.4–26.7] times, in favour of signals at sensor 1 than those at sensor 4 for four IPFRs. Thus, signal 1 is significantly less attenuated than signal 4.

The two graphs in Figure 12 and Figure 13 show, respectively, 1) time differences of appearances and 2) ratios of magnitudes between the extreme amplitudes and FPs in the first wave packets of corresponding signals at sensors for different IPFRs, which can be additionally influenced by reflected PD waves from the transformer's tank and active components.

When comparing signals 1, 2, 3, and 4 at the sensors 1–4, Figure 12 demonstrates that the PD wave reflections from the transformer's tank and active components result in different time differences of appearances between the signals' extreme amplitudes relative to FPs in the initial signals' packets, for each IPFR. Based on that, signals 2

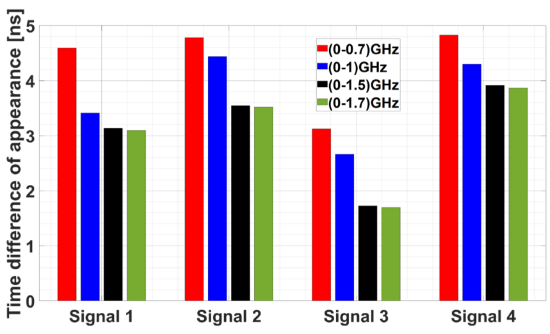

Figure 12: Time differences of appearances between the extreme amplitudes and FPs in the first wave packets of corresponding signals at UHF sensors for various IPFRs.

and 4 show the greatest number of PD wave reflections, whereas signal 3 shows the fewest. The time differences of appearances range from [3.86–4.83] ns for signal 4, [3.52–4.78] ns for signal 2, [3.10–4.59] ns for signal 1, and [1.69–3.12] ns for signal 3. As the IPFR increases, the time differences of appearances between the extreme amplitudes and FPs in the first packets of corresponding signals at the sensors decrease.

Figure 13 displays the ratios of magnitudes between the extreme amplitudes and the FPs in the first wave packets of corresponding signals at four UHF sensors for different IPFRs. For all IPFRs, it is evident that sensor four is where reflected waves from metal obstacles have the most significant influence on the signals. Therefore, the magnitudes' ratios at sensor four are significantly increased, in the range of [116.5–1004.7], with the maximum at IPFR of [0–0.7] GHz. For the other signals (at the first, second, and third sensors), the magnitudes' ratios are significantly smaller, i.e., in the ranges of [24.2–86.5], [22.7–35.5], and [23.3–61.2], respectively, with the minimum at IPFR of [0–1.7] GHz.

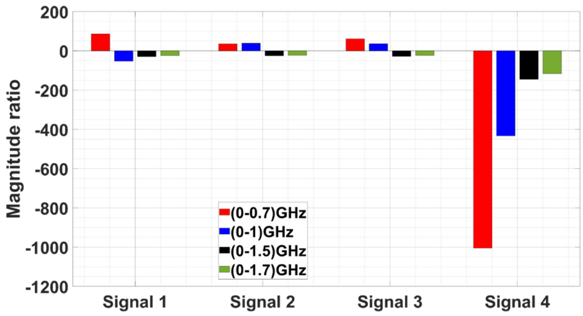

Figure 13: Magnitudes' ratios between the extreme amplitudes and FPs in the first wave packets of corresponding signals at sensors for different IPFRs.

Figures 14a-c and Figure 15 show, respectively, amplitude spectra of the output signals at sensors 1, 2, 3, and 4 in their first wave packets for different IPFRs of [0–0.7] GHz, [0–1] GHz, [0–1.5] GHz, and [0–1.7] GHz.

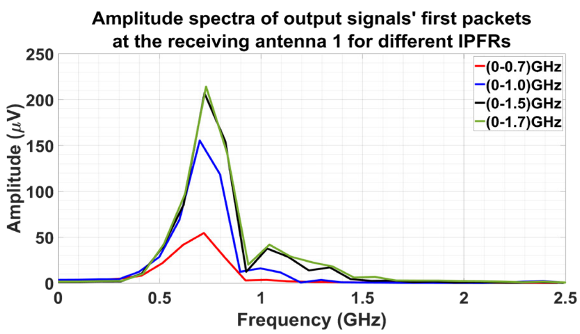

(a)

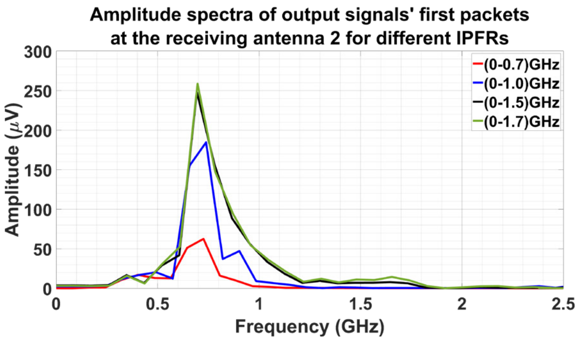

(b)

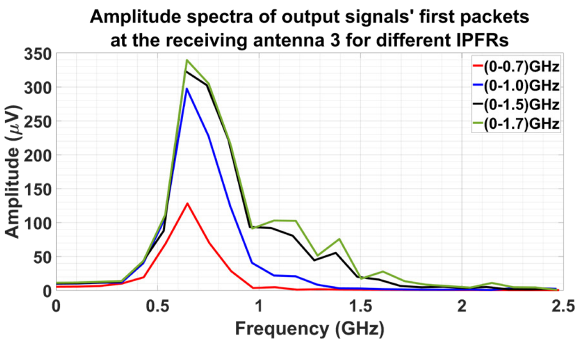

(c)

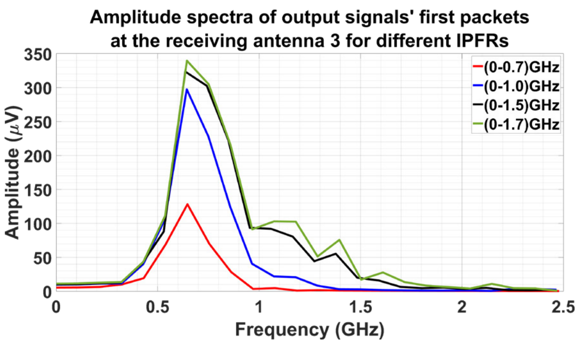

(d)

Figure 14: Amplitude spectra of the output signals recorded at sensors: (a) 1, (b) 2, and (c) 3 in their first wave packets lasting about [11.9–21.9] ns, [8.1–20.5] ns, [7.5–16.9] ns, respectively, for different IPFRs.

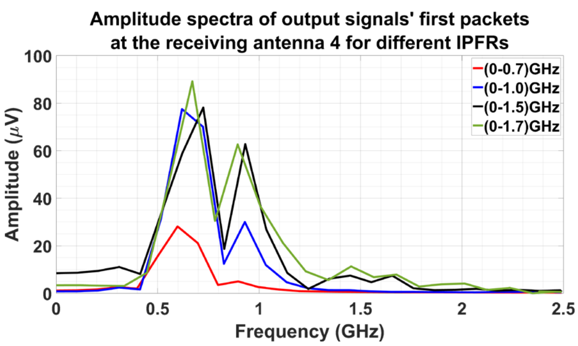

Figure 15: Amplitude spectra of the output signals recorded at sensor 4, in their first wave packets lasting about [12.4–22.4] ns, for different IPFRs.

Figure 16 displays the weighted average frequencies obtained from the corresponding amplitude spectra of the recorded signals at four UHF sensors for various IPFRs, allowing for a comparison of the amplitude spectra. The weighted average frequencies of the four received signals taken on the period of 2.5 GHz fall into the relatively smaller ranges [654–694] MHz, [724–749] MHz, [800–837] MHz, and [837–890] MHz, but with very different values from the corresponding weighted average frequencies of the output signals at PD source of 230.8 MHz, 423.2 MHz, 582.8 MHz, and 568.9 MHz, for IPFRs of [0–0.7] GHz, [0–1] GHz, [0–1.5] GHz, and [0–1.7] GHz. When compared to other IPFRs, the weighted average frequency of the output signal at the PD source for an IPFR of [0–1] GHz is the one that is closest to the half value of the corresponding IPFR of [0–1] GHz. For the used internal transformer structure and the IPFRs, it is clear that UHF sensors received signals at weighted average frequencies within a limited range [654–890] MHz. As a result, it is possible to conclude that the amplitude spectra of signals at four sensors are moved toward higher frequencies relative to the corresponding transmitting antenna's output signals, in all IPFRs.

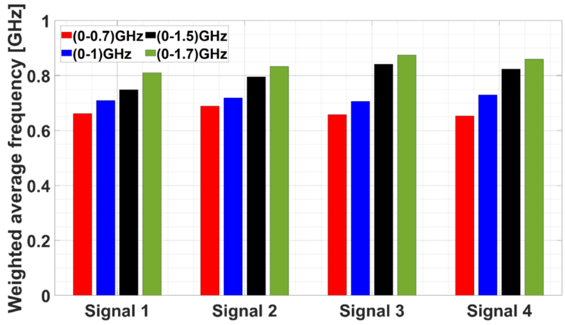

Figure 16: The weighted average frequencies of each recorded signal at four UHF sensors for various IPFRs.

According to Figure 4 in Section 1 showing the transmitting and receiving antennas' total efficiency versus frequency, the weighted average frequencies for the IPFRs of [0–0.7] GHz, [0–1] GHz, [0–1.5] GHz, and [0–1.7] GHz are, respectively, 613.4 MHz, 768.5 MHz, 937 MHz, and 1007.5 MHz. For IPFR of [0–1] GHz, the weighted average frequency range of output signals at sensors of [724–749] MHz is the nearest to the weighted average frequency of 768.5 GHz found from the total efficiency diagram of the transmitting and receiving antennas.

2.3. Analysing the average absolute location errors of the PD source for various IPFRs

Lastly, consideration should be given to how the various IPFRs affect the positioning of the PD source. Four sensors are sufficient for the accurate localisation of a PD source because four nonlinear equations with four unknown variables can be written and solved [6]. The FP method—which is based on figuring out the TDOAs between the FPs of the corresponding signals at three UHF sensors relative to the signal at the fourth reference UHF sensor—was employed. In this manner, by examining the recorded signals in Figures 9a-d, three TDOAs can be identified for each IPFR.

The four unknown values that need to be determined in the FP method are the TOA of the signal at the reference sensor and the three coordinates of the PD source position. These equations also contain fixed values, such as the 3D positions of the UHF sensors and the velocity of each UHF signal in mineral oil, which is 20.23 cm/ns. In general, everz two UHF sensors should be positioned far apart from each other to increase the possibility of getting a significant difference between the TOAs of PD signals at the sensors.

In Figure 17, the average absolute location errors of the PD source are obtained for various IPFRs. When using the [0–1] GHz IPFR, the average absolute location error was the lowest, at 4.45 cm. An IPFR of [0–0.7] GHz produced the highest average absolute location inaccuracy, 9.53 cm. At 1.7 GHz, the wavelength of the PD signal is 15.51 cm, and at 700 MHz, it is 24.17 cm. Because of the increasing diffractions and attenuations of the signals in the shortest paths from the PD source to the four sensors as IPFR decreases, it may have been expected that the absolute average location error in the simulation model depicted in Figure 1a would increase as IPFR decreases.

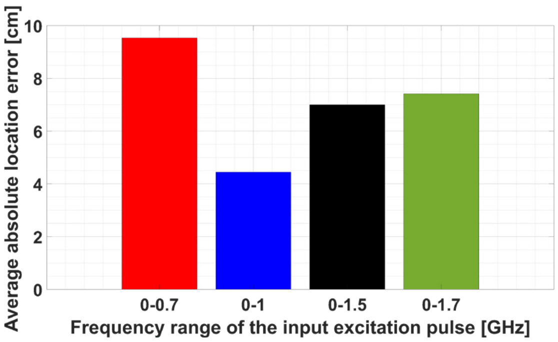

Figure 17: Calculated average absolute location errors of PD source in the cases of different IPFRs.

In these simulations, HFSS does adaptive passes until the Delta S falls below a set threshold. Due to computer RAM constraints, the minimum Delta S value that could have been set for the IPFRs [0–1.5] GHz and [0–1.7] GHz was 0.027. The average absolute location errors of the PD source were 7 cm and 7.42 cm, respectively. Computer RAM requirements increase with an increase in the IPFR. However, it was enabled to set Delta S at 0.02 for the IPFR of [0–1] GHz, which could have contributed to the improved accuracy of the PD source location result. The second reason could be more favourable TDOAs between FPs of the signals at sensors for [0–1] GHz IPFR. Despite setting Delta S in the range of [0.002–0.027] for IPFR of [0–0.7] GHz, the average absolute location error of the source remained the same and largest.

3. CONCLUSION

This paper provides a novel, detailed analysis of how the various IPFRs of the PD source, internal power transformer structure, and antenna properties affect the PD signals received at the four UHF sensors, as well as the assessments of PD source location in the power transformer. Four PD source IPFRs—[0–0.7] GHz, [0–1] GHz, [0–1.5] GHz, and [0–1.7] GHz—were employed in an attempt to obtain signals at UHF sensors that fall within the typical frequency range for PD signal detection.

In the power station or transformer station, the four UHF sensors installed on the power transformer would be able to detect PD signals more easily when IPFRs increase. It was demonstrated that the effects of PD wave reflections off the metal components of the transformer on the signals could be analysed using the time differences of appearances and the magnitudes' ratios between the extreme amplitudes and the FPs in the initial wave packets of recorded signals at the sensors. Since the magnitudes' ratios for signal 4 were the biggest for all IPFRs, it was determined that signal 4 was the one most affected by the reflected PD waves. Signal 3, which had the shortest time differences of appearances among all IPFRs, was demonstrated to be the one least affected by the reflected PD waves.

Based on the obtained amplitude spectra of the signals at the sensors, it was shown that the total antenna efficiency and the internal structure of the transformer affect them. In comparison to the amplitude spectra of the output signals from the transmitting antenna, the amplitude spectra of the signals recorded at four sensors were shifted toward higher frequencies for all IPFRs.

In terms of the position of the PD source, the IPFR of [0–1] GHz produced the best result. Four factors might have affected it: 1) the weighted average frequency range of received signals at the sensors was the nearest to the weighted average frequency found from the total efficiency diagram of the receiving antennas for the IPFR [0–1] GHz; 2) more favourable TDOAs between FPs of the signals at sensors for [0–1] GHz IPFR; 3) PD waves for the higher IPFR of [0–1] GHz are less diffracted and attenuated when they hit transformer metal obstacles on their way from a PD source to the sensors than PD waves for the lower IPFR of [0–0.7] GHz; 4) a smaller Delta S threshold was used in the simulation setup for the IPFR [0–1] GHz as opposed to the IPFRs [0–1.5] GHz and [0–1.7] GHz.

The main components of the transformer, such as the metal tank, three-limb magnetic core, and three-phase LV and HV windings (which were modelled as complex as possible), were all taken into consideration, and the simplifications and limitations of the transformer model were taken into account so as to have minimal effect on the results. Therefore, this makes it possible to compare the simulated results in this research with their real-world applicability. As demonstrated in the transformer simulation model presented in this paper, which incorporates the proposed PD source location, the localisation method applied in this paper could also be applied in practice (e.g., diagnostics, targeted inspection) to real power transformers with an unknown PD source location. One must have four UHF sensors built into the transformer, along with a four-channel digital oscilloscope with a high sampling rate to capture the signals on the sensors. The cables from the digital oscilloscope to the UHF sensors must be of the same length so as not to introduce additional delays between the signals.

REFERENCES

[1] Đ. Dukanac "Analysis of the Influence of Active Parts of the Power Transformer on the Propagation of Signals from Source of Partial Discharges to UHF Sensors (in Serbian)," Energy, Economy, Ecology, vol. XXIV, no. 1, 2022, pp. 74–80, doi: 1 0.46793/EEE22 -1 .74D

[2] D. Dukanac "Extraction of partial discharge signal in predominant VHF range in the presence of strong noise in power transformer," Electrical Engineering, vol. 105, no. 5, 2023, pp. 3001–3018, doi: 10.1007/s00202-023-01855-x

[3] S. Tenbohlen, C. P. Beura, W. Sikorski, R. A. Sánchez, B. A. de Castro, M. Beltle, P. Fehlmann, M. Judd, F. Werner, M. Siegel "Frequency Range of UHF PD Measurements in Power Transformers," Energies, vol. 16, no. 3, 2023, p. 1395, Electra N°321 , TB 861 , JWG A2/D1 .51 , 2022, pp. 1–1 0.

[4] S. Tenbohlen, C. P. Beura, W. Sikorski, R. A. Sánchez, B. A. de Castro, M. Beltle, P. Fehlmann, M. Judd, F. Werner, M. Siegel "Frequency Range of UHF PD Measurements in Power Transformers," Energies, vol. 16, no. 3, 2023, p. 1395, doi: 10.3390/en16031395.

[5] K. Schiewaldt, B. A. de Castro, J. A. Ardila-Rey, M. N. Franchin, A. L. Andreoli, S. Tenbohlen "Assessment of UHF Frequency Range for Failure Classification in Power Transformers," Sensors, vol. 24, no. 15, 2024, p. 5056.

[6] D. Dukanac "Application of UHF method for partial discharge source location in power transformers," IEEE Transactions on Dielectrics and Electrical Insulation, vol. 25, no. 6, December 2018, pp. 2266–2278, doi: 1 0.1 1 09/TDEI.201 8.006996

[7] C. P. Beura, M. Beltle, P. Wenger, S. Tenbohlen "Experimental Analysis of Ultra-High-Frequency Signal Propagation Paths in Power Transformers," Energies, vol. 15, no. 8, 2022, p. 2766, doi: 10.3390/en15082766.

[8] A. M. Ishak, M. D. Judd, W. H. Siew "A study of UHF partial discharge signal propagation in power transformers using FDTD modelling," in Proc. 45th International Universities Power Engineering Conference UPEC2010, 2010, 5 pp.

[9] D. Dukanac "Power Transformer Numerical Modelling to Locate Partial Discharge Source Using the UHF Technique," B&H Electrical Engineering, vol. 17, no. 2, 2023, pp 24–31, doi: 1 0.2478/bhee-2023-0009

[10] Đ. Dukanac "Influences of Reflections and Diffractions of Waves and the Modelled Source and UHF Sensors When Locating Partial Discharges in a Power Transformer (in Serbian)," Energy, Economy, Ecology, vol. XXVI, no. 3, 2024, pages 11–20, doi: 1 0.46793/EEE24-3.1 1D

[11] C. P. Beura, J. Wolters, S. Tenbohlen "Application of Pathfinding Algorithms in Partial Discharge Localization in Power Transformers," Sensors, vol. 24, no. 2, 2024, p. 685, doi: 1 0.3390/s24020685.

[12] F. Khodaveisi, H. Karami, M. Z. Karimpour, M. Rubinstein, F. Rachidi "Partial discharge localization in power transformer tanks using machine learning methods," Scientific Reports, vol. 14, Article no: 11785, 2024, 13 pp., doi: 10.1038/s41598-024-62527-9.

BIOGRAPHY

Đorđe Dukanac received a PhD in electrical and computer engineering from the School of Electrical Engineering, University of Belgrade, Serbia. His doctoral dissertation is titled "Application of UHF Sensors for Monitoring and Locating Partial Discharges in Power Transformers." He completed his previous magister's degree studies at the same faculty with an average grade of 10. His primary research interests include UHF sensors, detection, online monitoring, extraction, classification of UHF PD signals, and their source localisation in power transformers. In renowned scientific-professional national and international conferences and journals, he has presented 39 academic publications. Currently, his papers have 99 citations, nine recommendations, and an h-index of 4 in the ResearchGate database. He presented academic publications at international conferences in Austria, Belgium, Bosnia and Herzegovina, France, Serbia, the Netherlands, and Turkey. At conferences, he was a distinguished speaker and a reviewer; he received certificates of appreciation or recognition for presenting his publications and had the most notable paper and one of the notable contributions. In the IEEE Xplore database, his top scientific paper, "Application of UHF method for partial discharge source location in power transformers," has 1225 downloads. He is also cited in two patents registered in the United States and Europe. In the Springer Nature Link database, his outstanding scientific paper "Extraction of partial discharge signal in predominant VHF range in the presence of strong noise in power transformer" has 511 accesses. He is also an Editorial Board member of the Journal of Electrical and Electronic Engineering.